DEVELOPMENT OF A TSUNAMI FORECAST MODEL FOR PEARL HARBOR, HAWAII

L. Tang and C.D. Chamberlin

January 27, 2009

DRAFT

Contents

Abstract 6
1.0 Background and Objectives 6
2.0 Model Setup for Pearl Harbor, Hawaii 6
2.1 Forecast area and tsunami data 6
2.2 Historical data/tide gauges 2
.3 Bathymetry and Topography 5
2.4 Grid Setups 7
3.0 Validation and Verification for Historical and Simulated Tsunamis 11
3.1 Validation of the Pearl Harbor RIM for historical tsunamis 11
3.2 Verification of the Pearl Harbor SIM by the RIM 15
3.3 Robustness and stability tests 23
4.0 Summary 23
5.0 Acknowledgements 23
6.0 References 23
7.0 Appendix A 25
7.1 SIM *.in file for Pearl Harbor, HI 25

DRAFT

List of Tables

Table 1 Tsunami sources for fourteen historical tsunamis..... 4

Table 2 MOST setup of Pearl Harbor RIM and SIM 10

DRAFT

List of Figures

Figure 1 An aerial photo of Pearl Harbor 1

Figure 2 Bathymetric and topographic data source overview. 6

Figure 3 Grid setup for the Pearl Harbor RIM with resolution of (a) 36, (b) 6 and (c) 1/3 arc sec (10 m). 8

Figure 4 Grid setup for the Pearl Harbor SIM with resolution of (a) 120′, (b) 18′ and (c) 2 arc sec. 9

Figure 5 Virtual gauges in Pearl Harbor. 11

Figure 6 Validation of Pearl Harbor RIM with historical tsunami data recorded at Honolulu and Pearl Harbor tide gauge 14

Figure 7 Tsunami waveforms computed by the Pearl Habor SIM and RIM at Gauges 1 and 2 for the fourteen historical tsunamis. 16

Figure 8 Maximum water elevation computed by the RIM and SIM for the fourteen historical tsunamis. 22

DRAFT

Development of a Tsunami Forecast Model for Pearl Harbor, Hawaii

L. Tang and C.D. Chamberlin

DRAFT

Abstract

This report describes the testing of a tsunami forecast inundation model, named Stand-by Inundation Model (SIM), for Pearl Harbor, Hawaii, as a component of NOAA's tsunami forecast and warning system. The Pearl Harbor SIM was tested with fourteen historical tsunamis and a set of simulated T_{Mw} 9.3 tsunamis based on great subduction zone earthquakes in the Pacific. The SIM outputs were verified with numerical results from a reference inundation model (RIM) with higher resolution of 2/3 arc-second (20 m). The optimized SIM can provide a 4-hour local forecast of first wave arrival, amplitudes and reasonable inundation limit in minutes. It shows robust results for all test cases.

1.0 Background and Objectives

The NOAA Center for Tsunami Research (NCTR) at NOAA Pacific Marine Environmental Laboratory (PMEL) is developing a tsunami forecasting system known as Short-term Inundation Forecasting for Tsunamis (SIFT) for NOAA's Tsunami Warning Centers (Titov *et al*., 2005). The primary goal of the system is to provide NOAA's Tsunami Warning Centers with operational tools that combine real-time deep-ocean tsunami measurements from the Deep-ocean Assessment and Reporting of Tsunami (DART) buoys (Gonzalez *et al*., 2005; Bernard *et al.*, 2006, Bernard and Titov, 2007), with Method of Splitting Tsunami (MOST) model, a suite of finite difference numerical codes based on nonlinear long wave approximation, (Titov and Synolakis, 1998, Titov and Gonzalez, 1997, Synolakis, *et al*., 2007), to produce efficient forecasts of tsunami arrival time, heights, periods and inundation. To achieve accurate and detailed forecast on the likely impact of incoming tsunami on specific sites within certain time limits and to reduce false alarms, Stand-by Inundation Models (SIMs) are being developed for U.S. coastal communities that are potentially most at risk, and integrated as crucial components of the forecast system.

The report describes the development and testing of the Pearl Harbor SIM. The remainder of this report is organized as follows. Section 2 discusses the setups for the Pearl Harbor SIM and its Reference Inundation Model (RIM), including bathymetric and topographic data sources and model grid setups. Section 3 presents the model validation and verification for historical and simulated tsunamis. Summary and conclusions are provided in section 4.

2.0 Model Setup for Pearl Harbor, Hawaii

2.1 Forecast area and tsunami data

The main Hawaiian Islands are the younger and southern portion of the Hawaii Archipelago. From northeast to southwest, the islands form four natural geographic groups by shared channels and inter-island shelf, including (1) Ni'ihau, Ka'ula Rock, and Kauai, (Kauai complex) (2) Oahu, (3) Molokai, Maui, Lanai, and Kaho'olawe, (the Maui Complex), and (4) Hawaii (Smith, 1993). Pearl Harbor is located in the middle of Oahu's south shore and is the State's largest estuary. The forecast area covers the entire Pearl Harbor (Fig. 1).

DRAFT

Figure 1 An aerial photo of Pearl Harbor

The island of Oahu lies between Kauai, to the northwest, separated by the 115 km (72 mile) wide Kauai Channel, and Molokai, to the southeast, by the 42 km (26 mile) wide Kaiwi Channel. The island has very angular shoreline, with a narrow insular shelf surrounding most of the island (Shepard *et al*, 1950). On the southern side, the shelf terminates at a shallow depth around 50 m with a very steep slope beyond out to 300 m. Then the seafloor slopes more gently down to the 500 m depth of the Kaiwi Channel. On the southeast side of the Kaiwi Channel, Penguin Bank is the most extensive shallow shelf area in the Hawaii Islands. The 50-m isobath reaches over 42 km (26 miles) eastward from the west end of Molokai.

2.2 Historical data / tide gauges

Hawaii has a long history of distant-source tsunamis. The Pearl Harbor tide station at Fort Kamehameha, Bishop Point, was installed on 27 July 1948 and removed on 24 March 1987 (http://tidesandcurrents.noaa.gov/). Data from this tide station is available for the 1952 Kamchatka tsunami only. The nearby Honolulu tide stations recorded all of the fourteen tsunamis as summarized in Table 1.

Run-up records are available at 7 locations (Walker, 2004). Inside Pearl Harbor, the 1946 tsunami generated run-up ranging from 0.06 m (0.2 ft) at the Middle Loch to 0.5 m (1.5 ft) at the West Loch. The 1960 tsunami caused the most significant run-up, 3 m (9 ft) at both the open coast and Waikiki. There is no credible inundation data inside Pearl Harbor

DRAFT

No.	Tsunami ID	Area	Earthquake Date Time (UTC)	Location Lat (o)	Location Lon (o)	Sub. zone	Seismic moment magnitude (MW)	Tsunami moment magnitude (TMw)	Tsunami source
1	200708	Peru	2007.08.15 23:40:57	13.354S	76.509W	SASZ	8.0 (CMT)	8.1	14.1*a9+4.32*b9
2	200701	Central Kuril Is.	2007.01.13 04:23:20	46.272N	154.455W	KKJI	8.1 (CMT)	7.9	-3.64*b13
3	200611	Central Kuril Is.	2006.11.15 11:14:17	46.607N	153.230E	KKJI	8.3 (CMT)	8.1	14*a12+0.5*b12+2*a13+1.5*b13
4	200605	Tonga	2006.05.03 15:26:39	20.13N	174.164W	NZKT	8.0 (CMT)	8.0	6.6*b29
5	200311	Rat Is.	2003.11.17 06:43:07	51.13N	178.74E	AACC	7.7 (CMT)	7.8	12.81*b11
6	200309	Hokkaido	2003.09.25 19:50:06	42.4N	143.15E	KKJI	8.3 (CMT)	8.0	3.6m*(100x100km), 109#rake, 20#dip, 230#strike, 25m depth
7	200106	Peru	2001.06.23 20:33:14	16.14S	73.31W	SASZ	8.4 (CMT)	8.2	5.70*a15+2.90*b16+1.98*a16
8	199606	Andreanof	1996.06.10 04:04	51.478N	176.847E	AACC	7.9 (CMT)	7.8	2.40*a15+0.80*b16

DRAFT

9	199410	East Kuril Is.	1994.10.04 13:22:58.3	43.706N	147.328E	KKJI	8.3 (CMT)	8.1	9.00*a20
10	196403	Alaska	1964.03.28 03:36:14	61.04N	147.73W	AACC	9.2 (USGS)	29.0	Tang et al. (2006)
11	196005	Chile	1960.05.22 19:11:14	45.88S	76.29W	SASZ	9.5 (Kanamori & Cipar,1974)		
12	195703	Andreanof	1957.03.09 14:22:31	51.63N	175.41W	AACC	8.6 (USGS)	28.7	31.4*a15+10.6*a16+12.2*a17
13	195211	Kamchatka	1952.11.04 16:58:26.0	52.75N	159.50E	KKJI	9.0 (USGS)	28.7	
14	194604	Unimak	1946.04.01 12:28	52.75N	163.5E	AACC	8.5 (Lopez & Okal, 2006)	28.5	7.5*b23+19.7*b24+3.7*b25

1: Forecast tsunami source.

2: Preliminary result.

Table 1 Tsunami sources for fourteen historical tsunamis.

DRAFT

.3 Bathymetry and Topography

Tsunami inundation modeling requires accurate bathymetry in coastal area as well as high-resolution topography and bathymetry in the nearshore area. Digital elevation models (DEMs) were developed at medium resolution of 6 arc-second (180 m) covering all of the major Hawaiian Islands, and high resolution of 1/3 arc-second (10 m) covering the south Oahu area around Pearl Harbor. Both grids include topographic and bathymetric elevations. After compilation, the grids were resampled to produce the final modeling grids.

The source grids were compiled from several data sources; Figure 2 shows the spatial extent of each data source used. A detailed summary of the data sources can be found in Tang et al. (2006); in general, the data sources listed first superseded the sources listed later when they overlapped. The superseded datasets were used for comparison and verification.

DRAFT

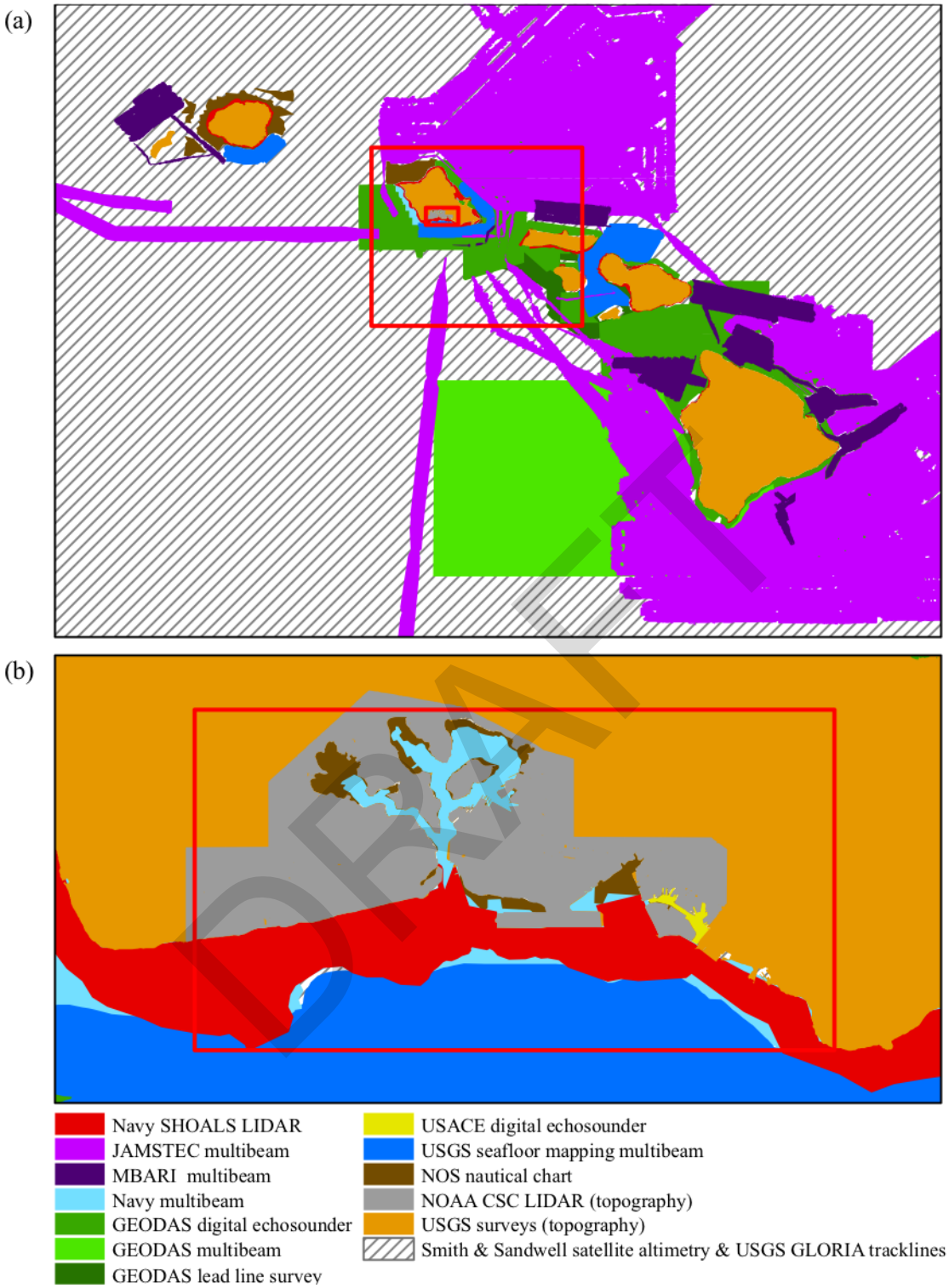

Figure 2 Bathymetric and topographic data source overview.

High-resolution, recent topographic LIDAR data was available for the area of interest around Pearl Harbor. SHOALS bathymetric LIDAR data were used in nearshore areas around several islands, providing excellent coverage of reef and shoreline regions.

High-resolution gridded datasets derived from multibeam surveys are available for many parts of the archipelago, and were used wherever available. In deep water where high-resolution multibeam data were not available, the grid was developed by interpolation of a combination of USGS GLORIA surveys and the Smith & Sandwell 2-minute (about 3.6 km in Hawaii) global seafloor dataset. These datasets were edited to remove individual points substantially different from nearby data.

Raw data sources were imported to ESRI ArcGIS-compatible file formats. Data values were converted, where necessary, to the WGS84 horizontal geodetic datum. In the point datasets, single sounding points that differed substantially from neighboring data were removed. Gridded datasets were checked for extreme values by examination of contour lines and, where available, by comparison between multiple data sources.

All selected input datasets were converted to the mean high water (MHW) vertical datum, when necessary, using offsets on the National Ocean Service tidal benchmark datasheet for the Honolulu tide station.

To compile the multiple data sources into a single grid, subsets of the source data were created in the priority order described above. A triangulated irregular network (TIN) was created from the vector point. Also added to the TIN were points taken from the edges of the gridded data regions to ensure a smooth interpolated transition between areas with different data sources. This TIN was linearly interpolated using ArcGIS 3D Analyst to produce intermediate 1/3 arc-second (10 m) and 6 arc-second (180 m) raster grids. The gridded datasets were then bilinearly resampled to these resolutions and overlaid on the intermediate grids

2.4 Grid Setups

By sub-sampling from the DEMs described in section 2.2, two sets of computational grids were derived, the Pearl Harbor Reference Inundation Model (RIM) (Fig. 3) and the Stand-by Inundation Model (SIM) (Figs. 4). Each set consists of three levels of telescoped grids with increasing resolution. The regional grids cover the major Hawaiian Islands and the coastal grids cover Oahu. Run-up and inundation simulations are calculated in nearshore grids over the study area. The solid boxes in red indicate boundaries of the nested grids. Grid details at each level and input parameters are summarized in Table 2.

DRAFT

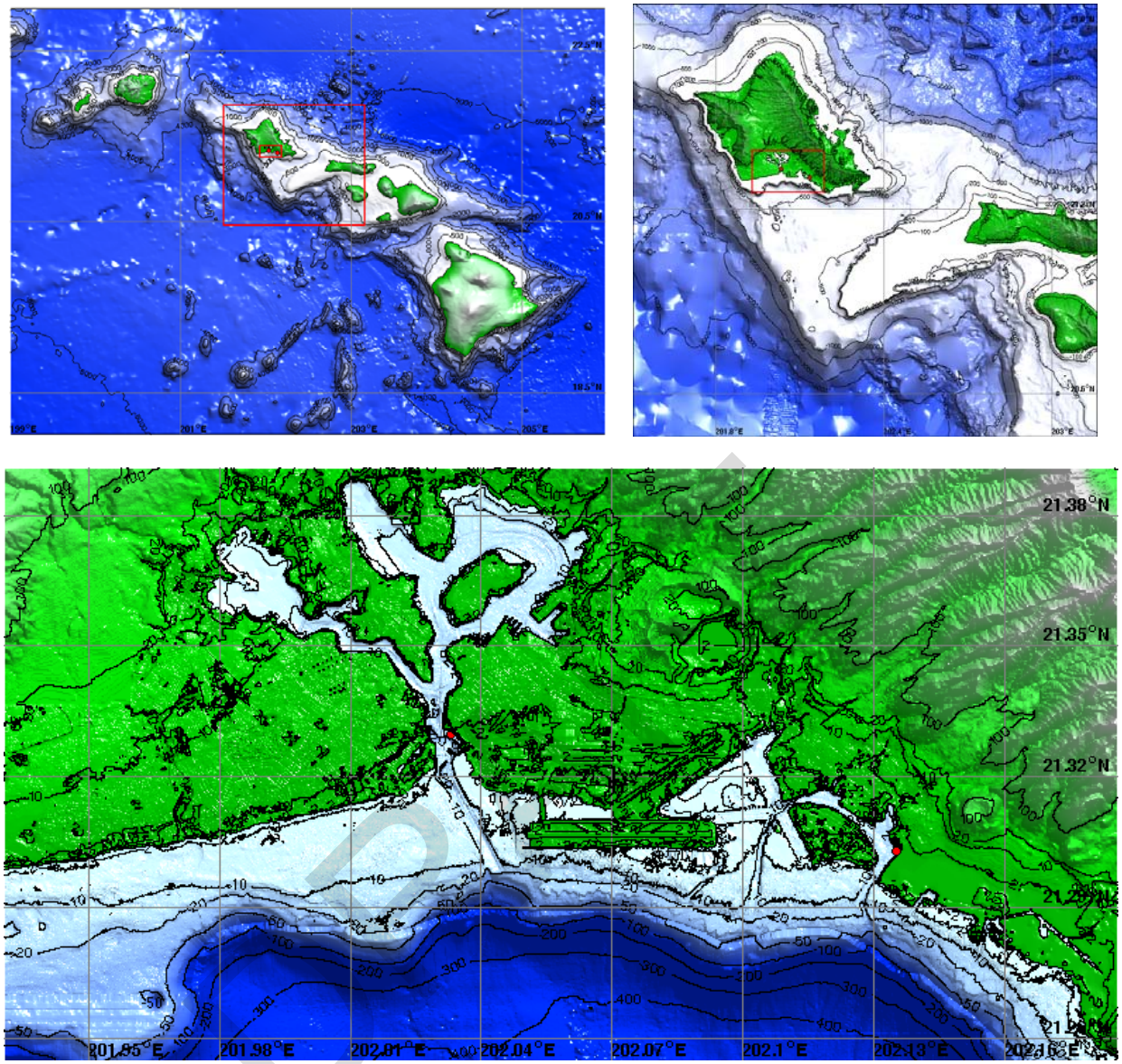

Figure 3 Grid setup for the Pearl Harbor RIM with resolution of (a) 36, (b) 6 and (c) 1/3 arc sec (10 m).

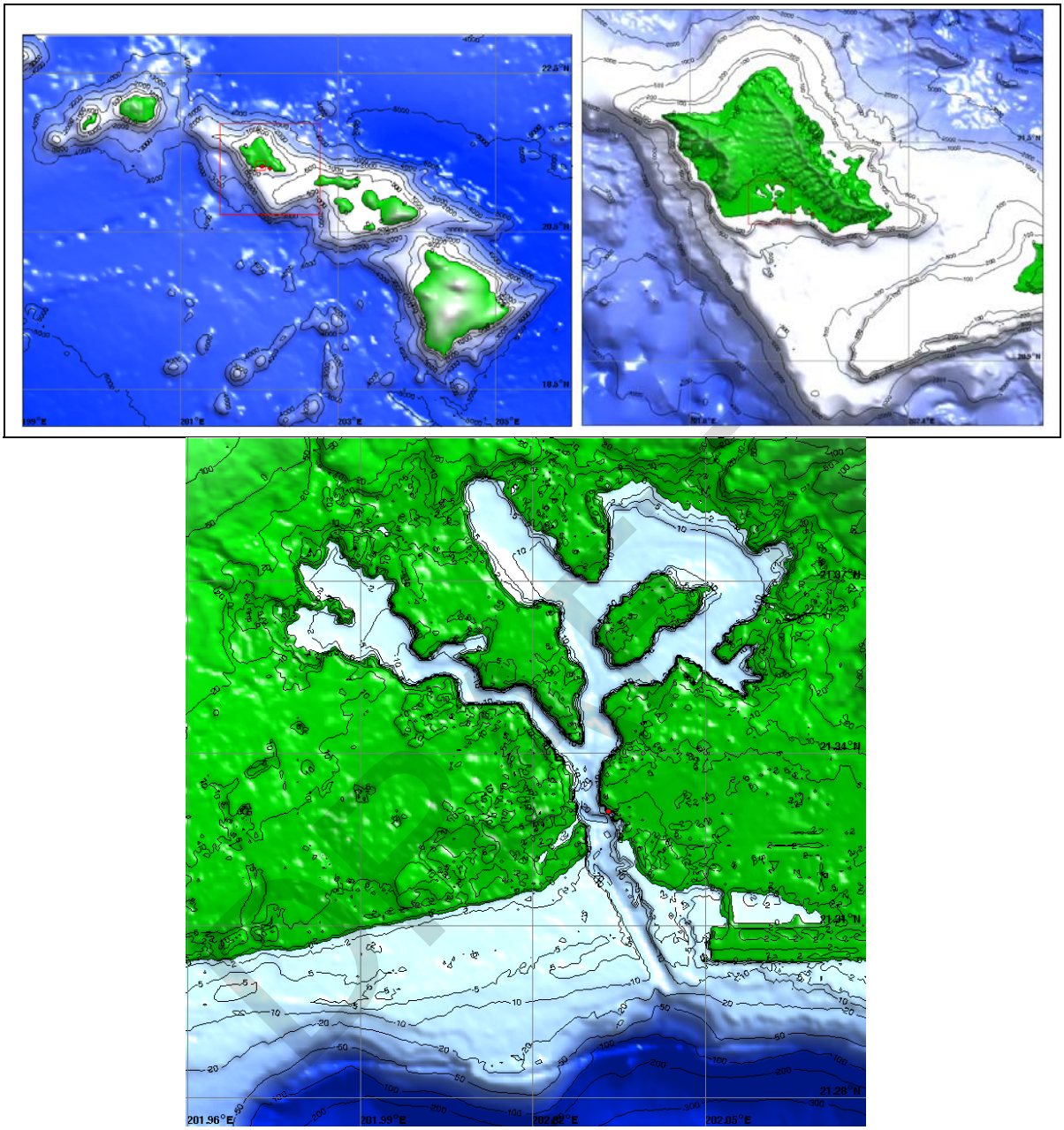

Figure 4 Grid setup for the Pearl Harbor SIM with resolution of (a) 120′, (b) 18′ and (c) 2 arc sec.

Grid	Region	Reference Inundation Model (RIM)			Stand-by Inundation Model (SIM)		
		Coverage Lon. [oE] Lat. [oN]	**Cell Size ["]**	**Time Step [sec]**	**Coverage Lon. [oE] Lat. [oN]**	**Cell Size ["]**	**Time Step [sec]**
A	Hawaii	199 - 205.98 18 - 23	36 (699 x 500)	2.4	199 - 205.9667 18.0317 - 22.9967	120 (210 x 150)	12.8
B	Oahu	201.503 – 203.163 20.458 - 21.867	6 (997 x 846)	0.48	201.5033 – 202.7683 20.7217 - 21.8667	18 (254 x 230)	2.4
C	Pearl Harbor	201.931 – 202.223 21.229 - 21.400	2/3 (1582 x 925)	0.24	201.9597 – 202.0781 21.275 – 21.395	2 (214 x 217)	0.8
Minimum offshore depth [m]			1		1		
Water depth for dry land [m]			0.3		0.1, 0.3		
Manning coefficient, Cm			0.03		0.03		
CPU time for a 4-hour simulation			~ 16 hours		**< 10 minutes**		

Table 2 MOST setup of Pearl Harbor RIM and SIM

DRAFT

For further investigation, 16 virtual gauges were systematically distributed in the forecast area (Fig. 5). Gauge 1 was located at the 2-m depth contour at the open coast. Gauge 2 represents the Ford Island nearshore. Gauges 3 to 16 record the waves propagating into the Pearl Harbor. Gauge 12 is under the Ford Island Bridge, close to the floating section.

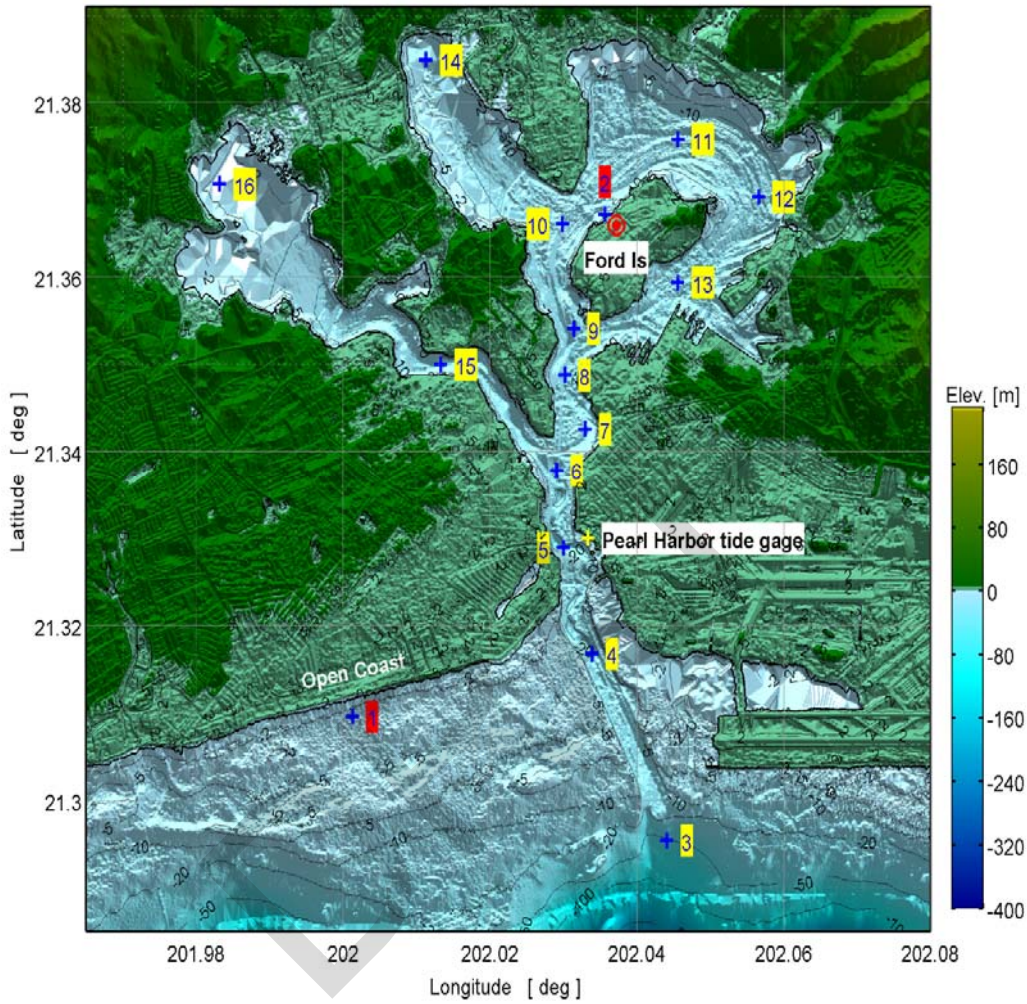

Figure 5 Virtual gauges in Pearl Harbor.

3.0 Validation and Verification for Historical and Simulated Tsunamis

The larger inundation area of the Pearl Harbor RIM covers the Honolulu tide station. In this section, first we validate the RIM with the historical tsunami records at the Honolulu tide station. Then we verify the SIM results by those computed from the high resolution RIM.

3.1 Validation of the Pearl Harbor RIM for historical tsunamis

Four recent and five destructive tsunamis from different subduction zones were employed in the model validation. Figure 6 shows the comparisons of model results and observations at Honolulu tide station.

The 3 May 2006 Tonga earthquake generated a tsunami that was detected about six hours later by two offshore tsunameters located to the south of the Hawaiian Islands. These data were combined with the model propagation database to produce the earthquake source by inversion (Tang et al. 2008). Very good model-observation agreement is obtained at Honolulu tide gauge, including the amplitudes, arrival time and wave period. It correctly models the 7th wave as the largest one (Fig. 6a).

The 17 November 2003 Rat Islands tsunami was detected by three tsunameters along the Aleutian Trench (Titov *et al.*, 2005). The model predictions also agree quite well with Honolulu tide gauge observations (Fig. 6b).

The shallow 25 September 2003 Hokkaido earthquake generated tsunami waves with an extraordinarily long period. Honolulu tide station recorded its first wave with a period of more than 48 minutes. Fig. 6c demonstrates that amplitudes, arrival time and period of first several waves of the wave train were correctly modeled.

No tsunameter data is available for the 23 June 2001 Peru tsunami. The tsunami source characteristics were derived from an inversion of the coastal Kahului tide gauge data using the Kahului SIM (Tang *et al.*, 2006). It gives good model-observation comparison at the Honolulu tide gauge (Fig. 6d).

The 28 March 1964 Alaska tsunami is the best documented of the historical events. Water-level data (Spaeth and Berkman, 1967) are available for ten of the SIM sites developed to date. The slip distribution of the source was then determined by inversion of data from two coastal tide stations, Kahului in Hawaii and Yakutat in Alaska, which gives a magnitude of 9.0. It produces excellent model comparison with observations at the Honolulu tide gauge (Fig. 6e).

The fault parameters of the 22 May 1960 Chile tsunami are taken from Kanamori and Ciper (1974). These give reasonable comparison of the wave amplitude and period to Honolulu tide gauge data (Fig. 6f). The computed arrival time is about 15 minutes earlier than the data.

The 9 March 1957 Andreanof Islands tsunami was one of the tsunamis with the longest aftershock zones ever recorded, at 1200 km (Johnson *et al*, 1994). The inversion using the Kahului and Crescent City SIMs gives a magnitude of 8.7. Fig. 6g shows reasonable comparison of computed and observed waveforms at Honolulu tide gauge.

Certain difficulties arise in the determination of the 4 November 1952 Kamchatka tsunami source. First, none of the SIMs available to date lies close to the earthquake source. Second, the Hawaiian SIMs with water level data are located at either the south or west shore of the islands, while the incoming waves were from the northeast. In addition, located perpendicular to the Kamchatka subduction zone, Hawaiian SIMs are in the least favorable arrangement for inversion since the travel times from the unit sources of the Kamchatka subduction zone to Hawaii do not vary much. Inversion using the Hilo tide gauge data gives a first estimate of the slip distribution. The wave amplitude was under-estimated at Honolulu gauge, but over-estimated at Pearl Harbor gauge (Fig. 6h and i).

In Hawaii, only the Honolulu tide station was available to record data for the 1 April 1946 tsunami. Inversion of the data gives a Magnitude of 8.5. Good comparison of model and observations was obtained (Fig. 6j). The third wave is the largest.

DRAFT

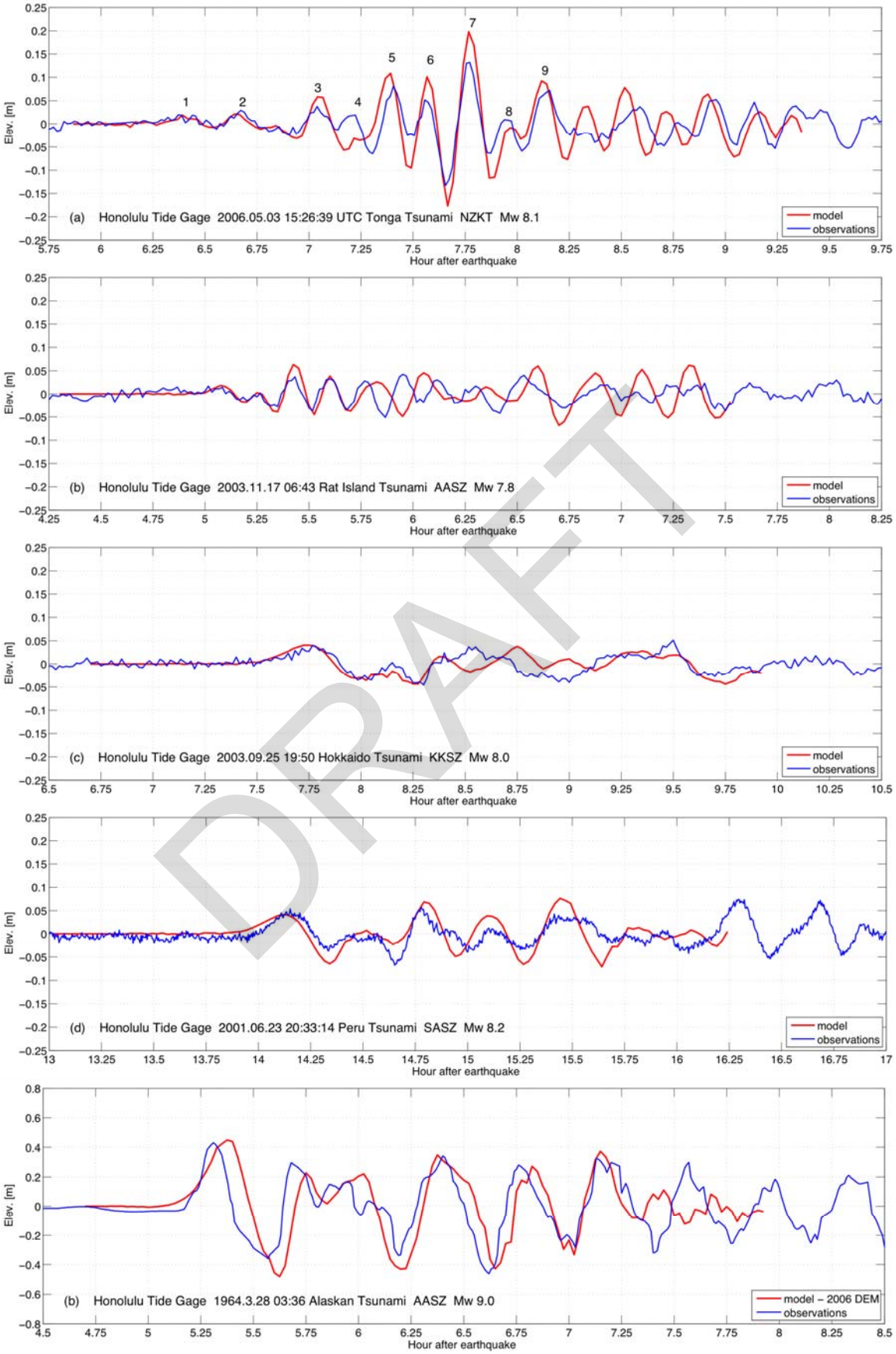
(a) Honolulu Tide Gage 2006.05.03 15:26:39 UTC Tonga Tsunami NZKT Mw 8.1
(b) Honolulu Tide Gage 2003.11.17 06:43 Rat Island Tsunami AASZ Mw 7.8
(c) Honolulu Tide Gage 2003.09.25 19:50 Hokkaido Tsunami KKSZ Mw 8.0
(d) Honolulu Tide Gage 2001.06.23 20:33:14 Peru Tsunami SASZ Mw 8.2
(b) Honolulu Tide Gage 1964.3.28 03:36 Alaskan Tsunami AASZ Mw 9.0
Elev. [m]
Hour after earthquake
model
observations
model – 2006 DEM

DRAFT

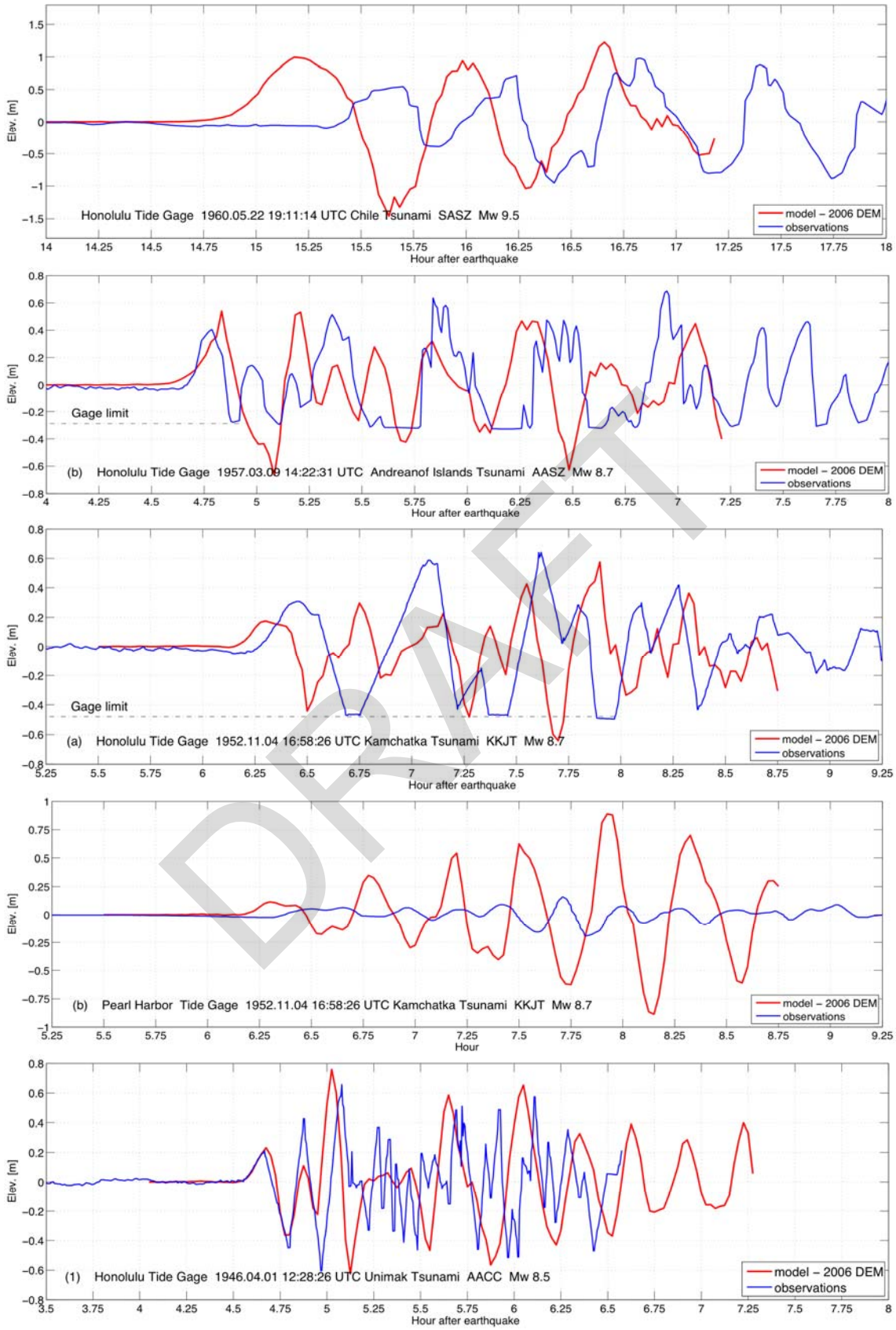

Figure 6 Validation of Pearl Harbor RIM with historical tsunami data recorded at Honolulu and Pearl Harbor tide gauge

DRAFT

3.2 Verification of the Pearl Harbor SIM by the RIM

Figure 7 compares the waveforms computed by the SIM and RIM at two locations, gauge 1 at the open coast and gauge 2 Ford Island nearshore inside Pearl Harbor. The SIM in general reproduces the tsunami time series as those computed by the high resolution RIM. With typical incident wave periods of 24 minutes or less at Gauge 1, the maximum wave amplitude at Ewa Beach is significantly larger than Ford Island (5 to 8 times). With longer period such as the approximately 32 minute waves for the 2001 Peru and 1964 Alaska tsunamis, resonance starts to appear inside Pearl Harbor. With the extraordinarily long periods of 2003 Hokkaido (48 minutes) and 1960 Chile (60 minutes) tsunamis, Gauge 2 clearly shows the influence of the characteristic resonance with a period around 96 minutes for Pearl Harbor. For these two events, the maximum wave amplitude at Ford Island is close or equal to that of the open coast.

DRAFT

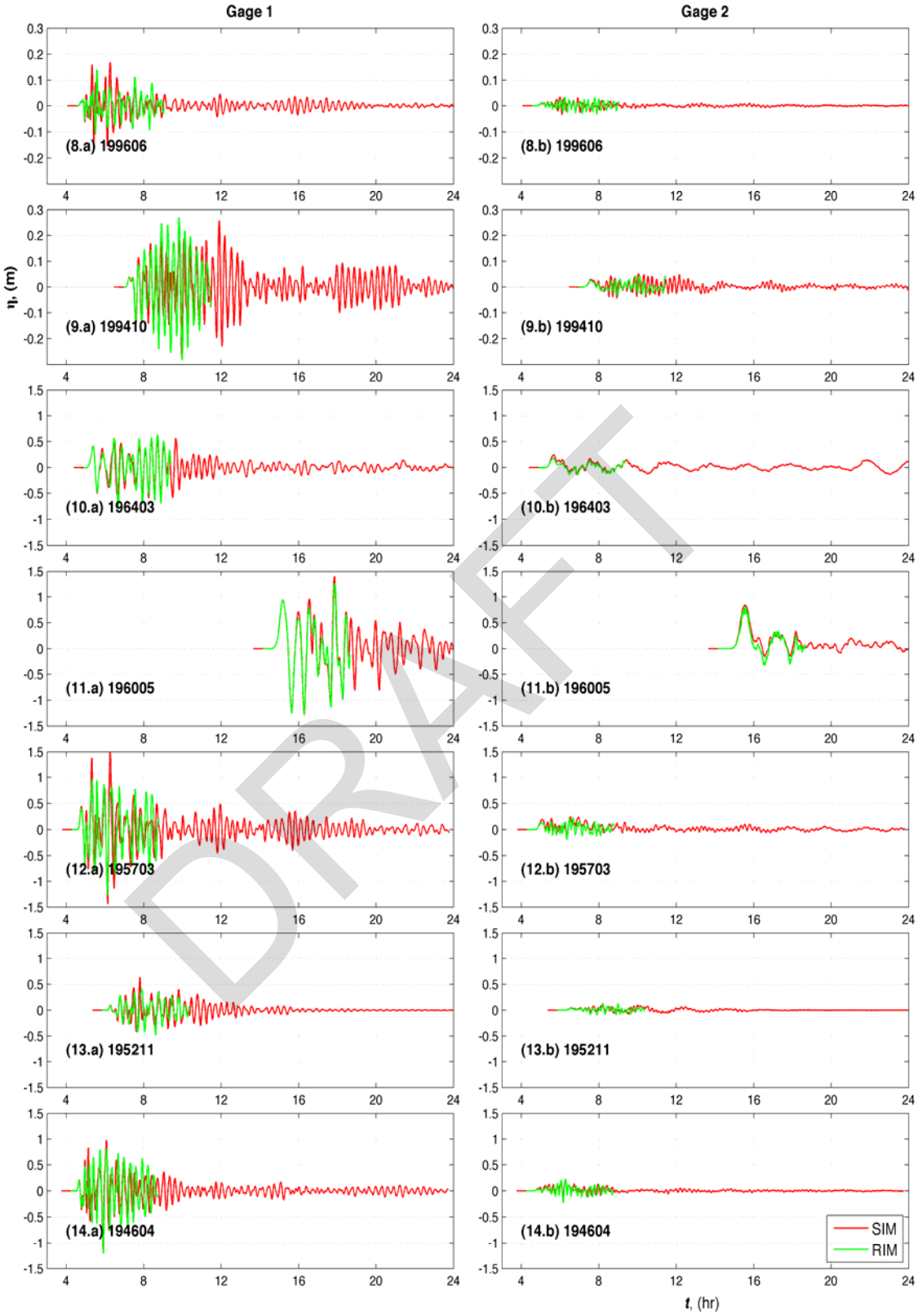

Figure 7 Tsunami waveforms computed by the Pearl Habor SIM and RIM at Gauges 1 and 2 for the fourteen historical tsunamis.

To explore the hazard wave conditions over the entire study area, computed maximum water elevation above MHW and maximum velocity of the fourteen tsunamis are plotted in Fig. 8. Both the RIM and SIM produced similar patterns and values. The offshore amplitudes up to 20 m water depth are small. However, the amplitude increases dramatically due to shoaling when the tsunami waves enter a nearshore area shallower than 20 m and even more so because of local shelf resonances and other coastal effects. This emphasizes the importance of using high-resolution inundation models, which resolve the local coast and harbor geometries, in order to achieve accurate tsunami amplitude forecasts for coastal communities.

DRAFT

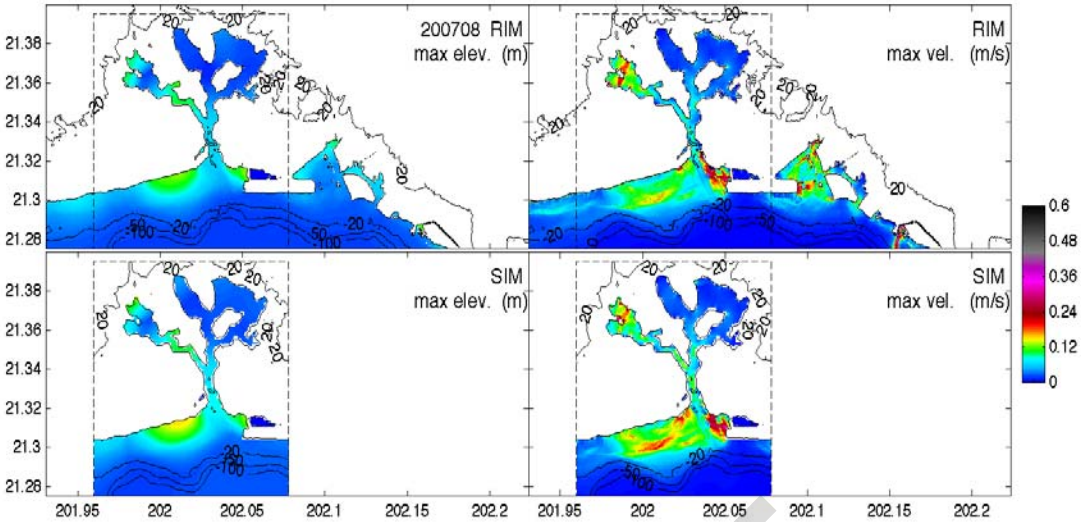
200708 RIM
max elev. (m)
RIM
max vel. (m/s)
SIM
max elev. (m)
SIM
max vel. (m/s)
0.6
0.48
0.36
0.24
0.12
0
21.38
21.36
21.34
21.32
21.3
21.28
201.95
202
202.05
202.1
202.15
202.2

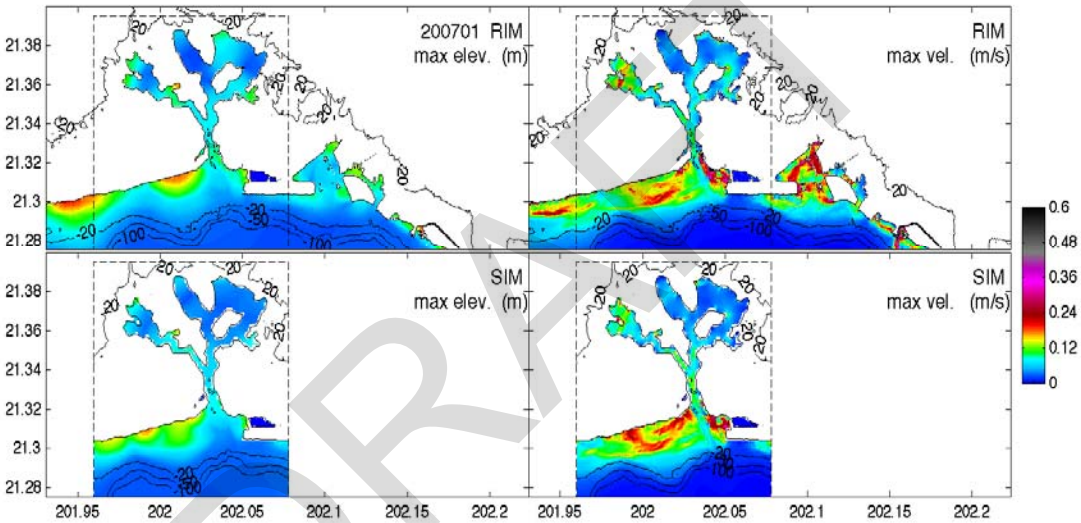
200701 RIM
max elev. (m)
RIM
max vel. (m/s)
SIM
max elev. (m)
SIM
max vel. (m/s)
0.6
0.48
0.36
0.24
0.12
0
21.38
21.36
21.34
21.32
21.3
21.28
201.95
202
202.05
202.1
202.15
202.2

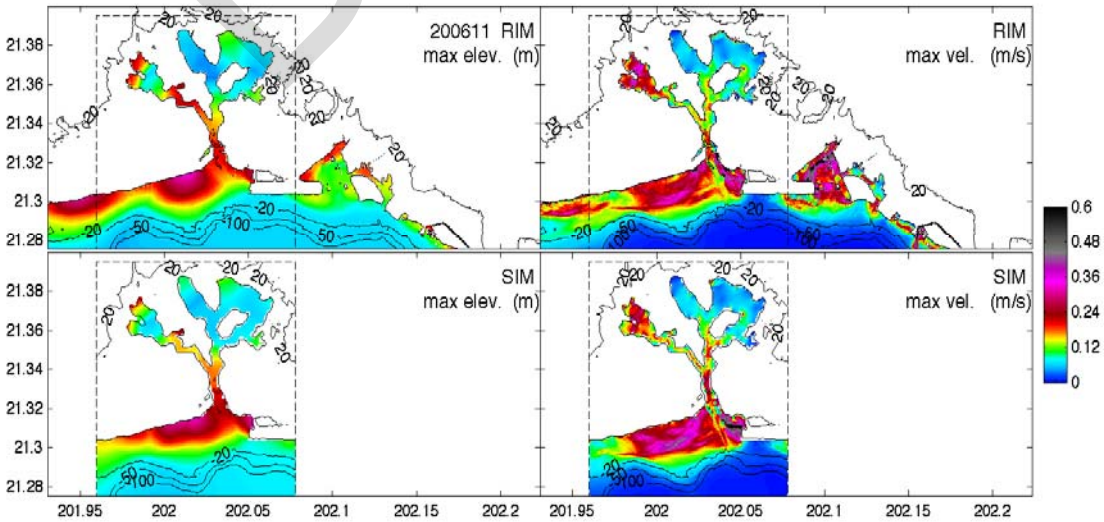
200611 RIM
max elev. (m)
RIM
max vel. (m/s)
SIM
max elev. (m)
SIM
max vel. (m/s)
0.6
0.48
0.36
0.24
0.12
0
21.38
21.36
21.34
21.32
21.3
21.28
201.95
202
202.05
202.1
202.15
202.2

DRAFT

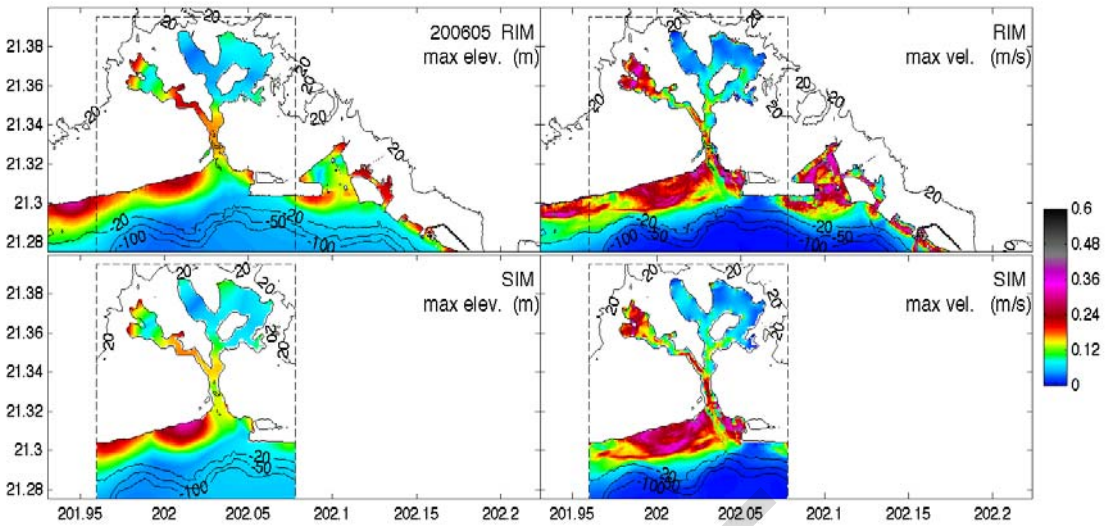
200605 RIM
max elev. (m)
RIM
max vel. (m/s)
SIM
max elev. (m)
SIM
max vel. (m/s)
0.6
0.48
0.36
0.24
0.12
0
21.38
21.36
21.34
21.32
21.3
21.28
201.95
202
202.05
202.1
202.15
202.2

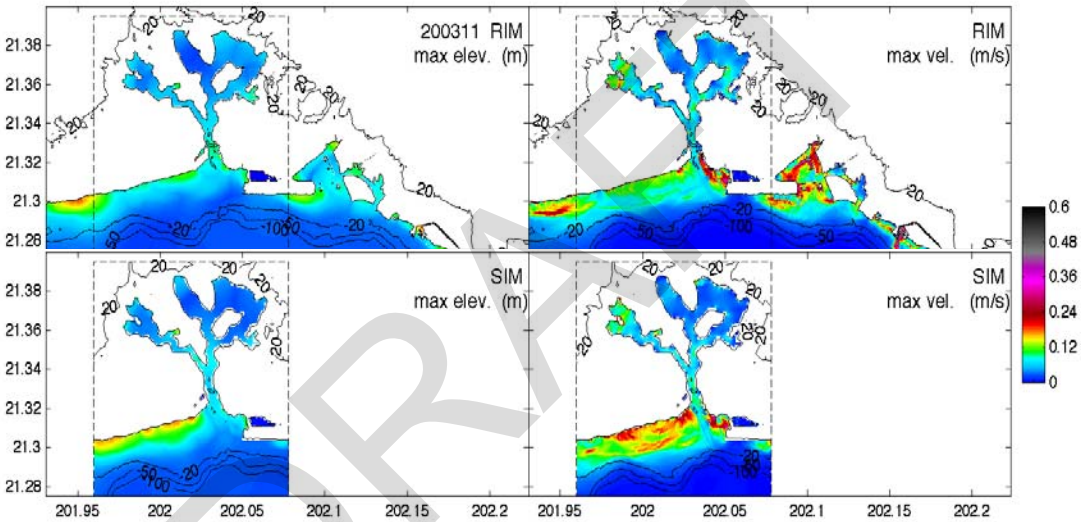
200311 RIM
max elev. (m)
RIM
max vel. (m/s)
SIM
max elev. (m)
SIM
max vel. (m/s)
0.6
0.48
0.36
0.24
0.12
0
21.38
21.36
21.34
21.32
21.3
21.28
201.95
202
202.05
202.1
202.15
202.2

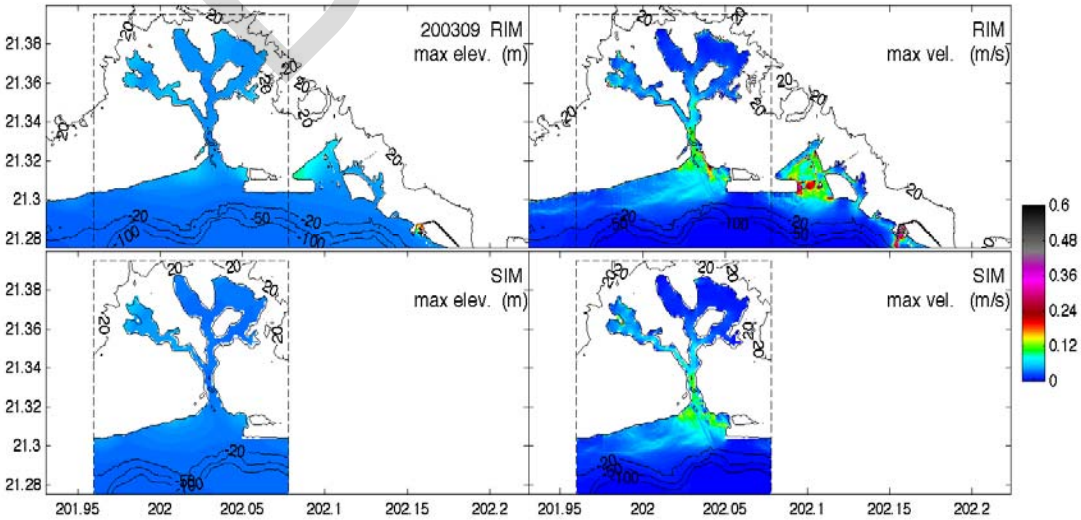
200309 RIM
max elev. (m)
RIM
max vel. (m/s)
SIM
max elev. (m)
SIM
max vel. (m/s)
0.6
0.48
0.36
0.24
0.12
0
21.38
21.36
21.34
21.32
21.3
21.28
201.95
202
202.05
202.1
202.15
202.2

DRAFT

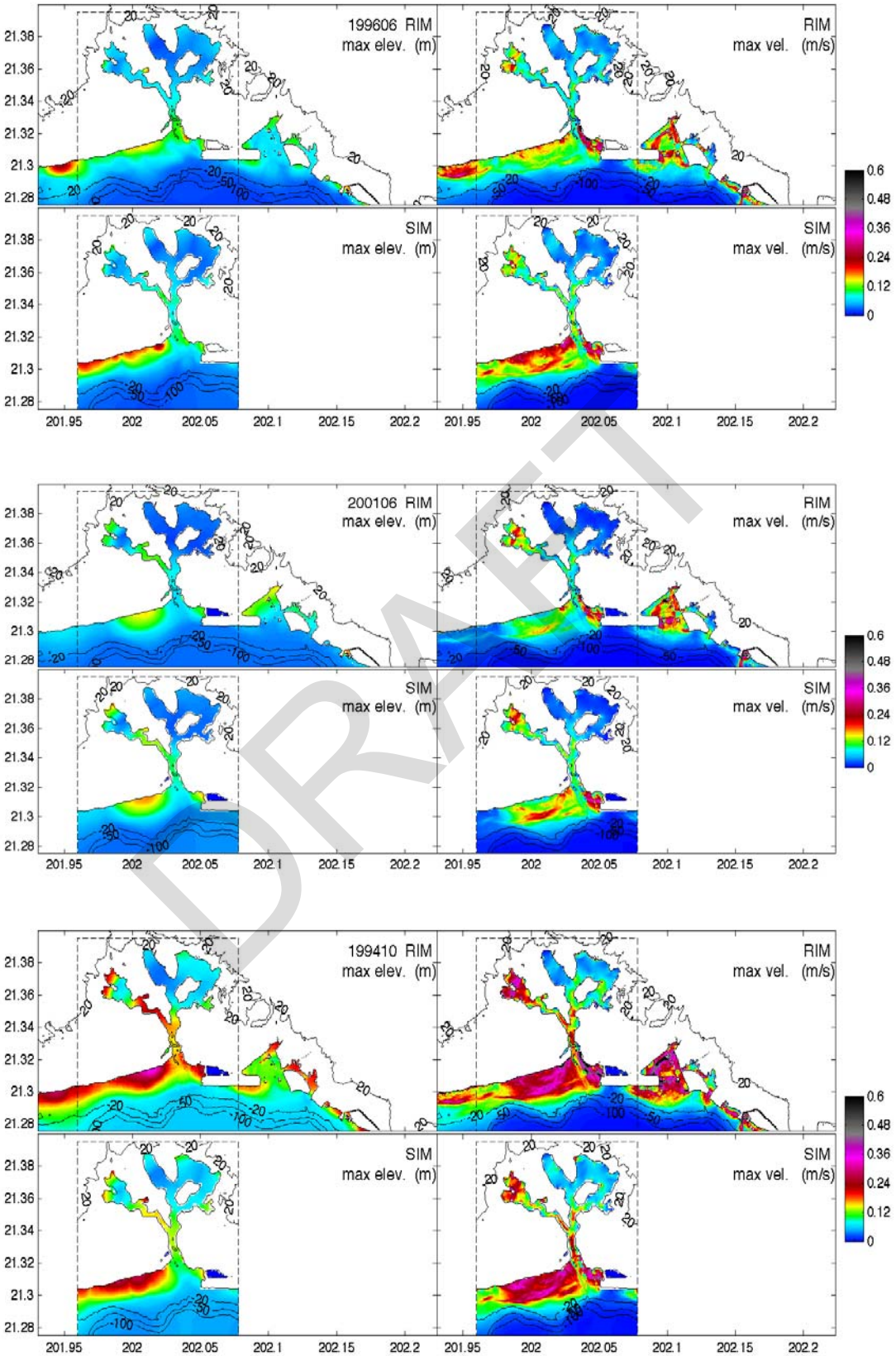
199606 RIM
max elev. (m)
RIM
max vel. (m/s)
SIM
max elev. (m)
SIM
max vel. (m/s)
200106 RIM
max elev. (m)
RIM
max vel. (m/s)
SIM
max elev. (m)
SIM
max vel. (m/s)
199410 RIM
max elev. (m)
RIM
max vel. (m/s)
SIM
max elev. (m)
SIM
max vel. (m/s)
0.6
0.48
0.36
0.24
0.12
0
21.38
21.36
21.34
21.32
21.3
21.28
201.95
202
202.05
202.1
202.15
202.2

DRAFT

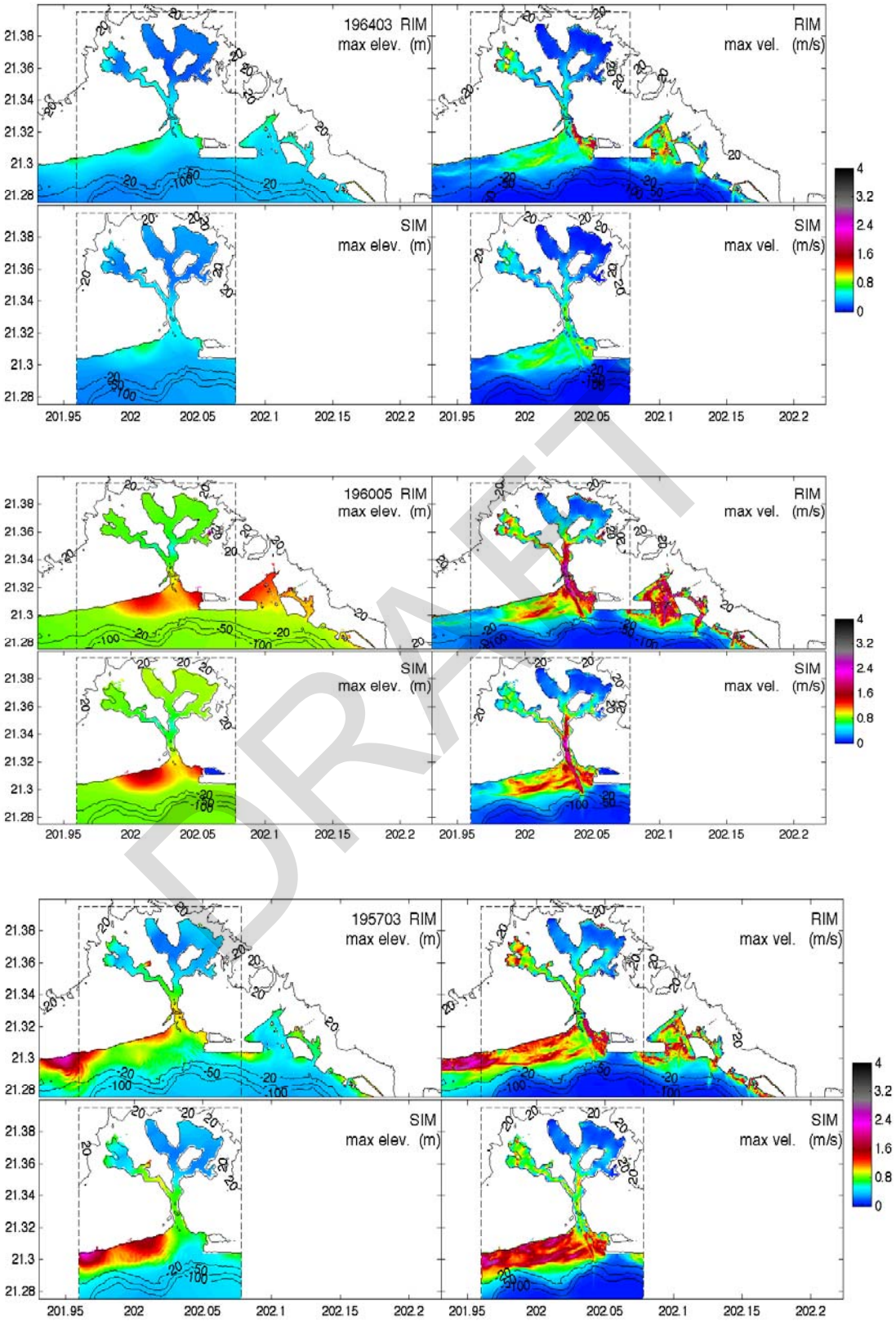
196403 RIM
max elev. (m)
RIM
max vel. (m/s)
SIM
max elev. (m)
SIM
max vel. (m/s)
196005 RIM
max elev. (m)
RIM
max vel. (m/s)
SIM
max elev. (m)
SIM
max vel. (m/s)
195703 RIM
max elev. (m)
RIM
max vel. (m/s)
SIM
max elev. (m)
SIM
max vel. (m/s)
21.38
21.36
21.34
21.32
21.3
21.28
201.95
202
202.05
202.1
202.15
202.2
4
3.2
2.4
1.6
0.8
0

DRAFT

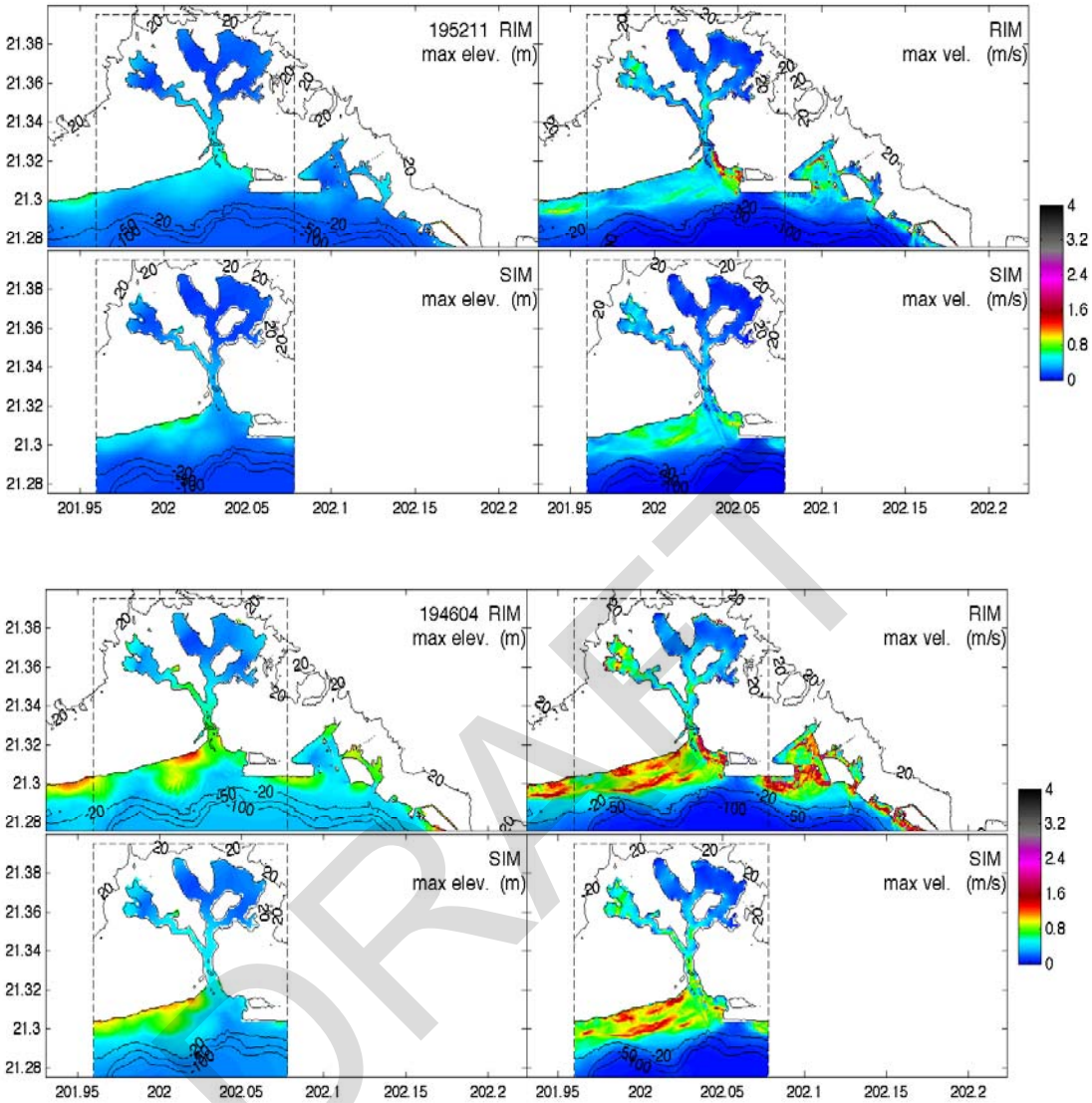

Figure 8 Maximum water elevation computed by the RIM and SIM for the fourteen historical tsunamis.

DRAFT

3.3 Robustness and stability tests

Recorded historical tsunamis provide only a limited number of events, from limited locations. More comprehensive test cases of destructive tsunamis with different directionalities are needed to check the stability and robustness for SIMs. The same set of 18 simulated T_{Mw} 9.3 tsunamis as in Tang et al. (2008) was selected here for further examination. SIM results are compared with those from the high resolution RIM in Figs. 9 and 10. Both models were numerically stable for all of the scenarios. Waveforms computed by the SIM agree well with those from the RIM (Fig. 9). SIM and RIM compute similar maximum water elevation and inundation in the study area (Fig. 10). These results indicate the Kahului SIM is capable of providing robust and stable predictions of long duration for Pacific-wide tsunamis.

Tsunami waves in the study area vary significantly for the 18 T_{Mw} 9.3 scenarios. These results show the complexity and high nonlinearity of tsunami waves in the nearshore, which again demonstrate the value of SIMs for providing accurate site-specific forecast details.

4.0 Summary

A Stand-by Inundation Model (SIM) was developed for the Pearl Harbor, Hawaii. The computational grids for the Pearl Harbor SIM were derived from the best available bathymetric and topographic data sources. The model was tested with 14 historical tsunamis and different scenarios of simulated 9.3 tsunamis based on subduction zone earthquakes in the Pacific. The SIM outputs are compared to both historical water level data and numerical results from a reference inundation model (RIM) of higher resolution. The optimized SIM can provide a 4-hour local forecast of first wave arrival, amplitudes and reasonable inundation limit in minutes. It shows robust results for all test cases.

5.0 Acknowledgements

Thanks to Jean Newman for assistance with the propagation database; and Ryan L. Whitney for comments and editing.

This research is funded by the NOAA Center for Tsunami Research (NCTR) 2985. This publication is partially funded by the Joint Institute for the Study of the Atmosphere and Ocean (JISAO) under NOAA Cooperative Agreement No. NAxxxxx, Contribution #xxxx.

6.0 References

Gica, E., M.C. Spillane, V.V. Titov, C.D. Chamberlin, and J.C. Newman (2008), Development of the forecast propagation database for NOAA's Short-Term Inundation Forecast for Tsunamis (SIFT), *NOAA Tech. Memo. OAR PMEL-139*, 89 pp.

González, F.I., E.N. Bernard, C. Meinig, M.C. Eble, H.O. Mofjeld, and S. Stalin (2005), The NTHMP tsunameter network, *Natural Hazards*, *35*, 25–39.

DRAFT

Spaeth, M.G. and S.C. Berkman, (1965), *The tsunami of March 28, 1964, as recorded at tide stations*, U.S. Coastal and Geodetic Survey Publication. Rockville, Maryland: U.S. Coast and Geodetic Survey, 59 pp.

Synolakis, C.E., E.N. Bernard, V.V. Titov, U. Kânoğlu, and F.I. González (2007), Standards, criteria, and procedures for NOAA evaluation of tsunami numerical models. *NOAA Tech. Memo. ERL PMEL-135*, 55 pp.

Tang, L., C. Chamberlin, E. Tolkova, M. Spillane, V.V. Titov, E.N. Bernard, and H.O. Mofjeld (2006): Assessment of potential tsunami impact for Pearl Harbor, Hawaii. NOAA Tech. Memo. OAR PMEL-131.

Tang, L., C. Chamberlin and V.V. Titov, (2008), Developing tsunami forecast inundation models for Hawaii: procedures and testing, *NOAA Tech. Memo., OAR PMEL -141*, 46 pp.

Tang, L., V. V. Titov, Y. Wei, H. O. Mofjeld, M. Spillane, D. Arcas, E. N. Bernard, C. Chamberlin, E. Gica, and J. Newman (2008), Tsunami forecast analysis for the May 2006 Tonga tsunami, J. Geophys. Res., 113, C12015, doi:10.1029/2008JC004922.

Titov, V.V. (2008), Chapter 12 Tsunami forecasting, In *The SEA*, 15, edited by E. Bernard and A. Robinson, Harvard Univ. Press, Cambridge, Mass., in press.

Titov, V.V., and F.I. González (1997), Implementation and testing of the Method of Splitting Tsunami (MOST) model, *NOAA Tech. Memo. ERL PMEL-112*, 11 pp.

Titov, V.V., H.O. Mofjeld, F.I. González, and J.C. Newman (2001), Offshore forecasting of Alaskan tsunamis in Hawaii, In *Tsunami Research at the End of a Critical Decade*, edited by G.T. Hebenstreit, Kluwer Academic Publishers, Amsterdam, 75–90.

Titov, V.V., F.I. González, E.N. Bernard, M.C., Eble, H.O. Mofjeld, J.C. Newman, and A.J. Venturato (2005), Real-time tsunami forecasting: challenges and solutions, *Natural Hazards*, *35*(1), 41–58.

Titov, V.V., and C.S. Synolakis (1998), Numerical modeling of tidal wave runup. J. Waterw. Port Coast. Ocean Eng., ASCE, 124(4), 157–171.

DRAFT

7.0 Appendix A

7.1 SIM *.in file for Pearl Harbor, HI

```
0.0001 Minimum amplitude of input offshore wave (m):
1      Input minimum depth for offshore (m)
0.3    Input "dry land" depth for inundation (m)
0.001  Input friction coefficient (n**2)
1      runup flag for grids A and B (1=yes,0=no)
300.0  blowup limit
0.8    Input time step (sec)
36000  Input amount of steps
16     Compute "A" arrays every n-th time step, n=
3      Compute "B" arrays every n-th time step, n=
48     Input number of steps between snapshots
0      ...Starting from
1      ...Saving grid every n-th node, n=
```

DRAFT